

Effect of graphite morphology on water absorption and fatigue properties of biopolyamide matrix composites

Patrycja Bazan^{1*}, Paulina Majewska¹, Cezary Drenda², Kristofer Gunnar Paso³

¹ Faculty of Material Engineering and Physics, Cracow University of Technology, Warszawska 24, 31-155 Krakow, Poland

² Faculty of Mechanical Engineering and Robotics, Department of Machine Design and Maintenance, AGH University of Krakow, al. A. Mickiewicza 30, 30-059 Krakow, Poland

³ Department of Chemical Engineering, Norwegian University of Science and Technology, 7034, Trondheim, Norway

* Corresponding author's e-mail: patrycja.bazan@pk.edu.pl

ABSTRACT

This study examines graphite morphology's impact on water absorption and fatigue properties of biopolyamide-based composites. Graphite is incorporated in flake and expanded forms. Flake graphite consists of thin, flat flakes with layered crystalline structure, high purity, and thermal/electrical conductivity. Expanded graphite, produced by intercalating flake graphite with acid and heating, has a worm-like, porous structure with low density and high surface area. The methodology includes density measurement, water absorption testing, and mechanical assessments. Fatigue behavior is assessed using the Lehr method, with mechanical hysteresis loops analyzed. Graphite enhances mechanical performance of biopolyamides. The modulus of elasticity increases by 40% for material modified with flake graphite, while expanded graphite presents a 10% increase. However, tensile strength decreases by a few percent with flake graphite and 30% with expanded graphite. Water absorption is reduced by up to 20% due to graphite's lamellar structure. Graphite composites show increased fatigue and dynamic creep resistance, with fatigue strength increasing 30% relative to matrix material. Expanded graphite influences friction behavior under low-load conditions. Graphite-filled composites maintain mechanical properties upon thermal aging, while neat BioPA degrades significantly. After accelerated thermal aging, unmodified material presents a 30% and 70% decrease in elastic modulus and tensile strength, while flake graphite composites shows a 20% and 15% decrease, respectively. The findings demonstrate graphite morphology's role in improving tribological properties, moisture uptake and fatigue resistance.

Keywords: biopolyamide composites, graphite morphology, water absorption, fatigue resistance, thermal aging.

INTRODUCTION

Polyamides (PA) and biopolyamides have distinct characteristics that differentiate them in terms of properties and applications. Bio-based polyamides, derived from biological sources, offer improved sustainability and environmental benefits in comparison to conventional polyamides [1], Bio-polyamides are less crystalline and more flexible, making them suitable for applications such as printing inks, varnishes and heat-sealable coatings [1]. Biopolyamides can be synthesized by various methods, including

condensation reactions of di-amines and bio-derived di-carboxylic acids, or ring-opening polymerization of lactams [2]. In terms of mechanical and thermal properties, biopolyamides show superior properties compared to conventional polyamides. For example, biopolyamides have higher tensile strength and thermal stability than petrochemical polyamides, making them suitable for high-performance applications [3–5]. The synthesis of identical polyamide materials can be achieved whether the monomer is derived from petroleum or biological sources,

contingent upon monomer purification. However, from an environmental perspective, the shift from petrochemical-based to bio-based polyamide production is significant. Bio-based polyamides use renewable resources and demonstrate better life-cycle attributes, including reduced carbon emissions and potential biodegradability. [6]. In addition, current research focuses on the development of environmentally friendly composites and nanocomposites based on biopolyamides and natural fillers, emphasizing the sustainability of these materials [7]. On the other hand, conventional polyamides such as nylon are widely used in various industries [8]. Biopolyamide composites are in high demand in various fields due to their potential in sustainable and high-performance applications. Scientists investigate various aspects of biopolyamide composites, including the effect of fibre type on microstructure and mechanical parameters [9], synthesis and modification of modern materials based on biopolyamides [7] and use of polyamides from renewable sources as matrices for short-fibre reinforced biocomposites. Research focused on improving the properties of biopolyamide composites by incorporating different fibres such as glass [10], basalt, wood [11, 12]. In addition, preparation of biopolyamide nanocomposites using techniques such as melt mixing and in situ polymerisation was investigated [13]. Environmentally friendly composites were developed using partially bio-based polyamides and natural fillers such as halloysite nanotubes [14]. In addition, compatibilisation of starch particles with biopolyamides was investigated to improve sustainability and adjust the start-up temperature [15]. Researchers also delved into structural optimisation of biopolyamides to increase strength and resistance in contact with food chemicals, and the preparation of cured biopolyamides for impact-resistant hybrid composites [16, 17]. However, scientists are not only interested in strength or thermal properties, but also in tribological properties. These additives play a key role by offering increased lubricity, reduced coefficients of friction and lower wear rates.

The primary wear mechanism of polymer materials during dry gliding is adhesive wear, affected by surface work and sliding surface durability. This wear depends on transfer layer abrasion and replacement rates. To improve tribological properties of polymer-metal pairs,

both external lubricants (oil, grease) and internal lubricants are used. External lubricants require regular replacement and can be unevenly distributed, increasing costs. Internal lubricants in polymers can improve wear and friction resistance by replacing fast-wearing polymers and lubricated metals, while offering benefits like weight reduction, reduced noise, lower costs, and elimination of corrosion [18].

Internal lubricants are used to reduce coefficients of friction between polymer and metal surfaces, increase wear resistance, improve flow characteristics and polymer properties. Researchers have developed a wide range of internally lubricated polymers with various lubricants such as polytetrafluoroethylene (PTFE), silicone oil [19], aramid fiber [20], graphite and molybdenum disulfide (MoS_2), etc., ensuring less wear and lower coefficient of friction, and thus longer service life of the parts. Self-lubricating polymer materials can be produced by adding a small amount of silicone fluid directly to molten thermoplastic. Commonly used internal lubricants include waxes, fatty acids, metal stearates, aramid, silicone, graphite, and molybdenum disulfide [21, 22].

Graphite, an allotropic form of carbon, has a layered structure of two-dimensional hexagonal units, with carbon atoms forming honeycomb-like arrangements through covalent bonds. These parallel layers are held by van der Waals forces. Graphite exhibits good lubrication, electrical conductivity along layers, high strength, chemical stability, thermal conductivity, and shock resistance [23]. Research on the introduction of graphite into polymer composites is aimed at improving the conductive properties of the material as well as improving tribological properties [24–26].

Polymer composites with graphite powder as a solid lubricant were developed by Difallah et al. using hot-compression molding. The matrix was acrylonitrile butadiene styrene (ABS). Mechanical studies showed graphite particles negatively affected sample stretching, but reduced the friction coefficient, with optimal results at 7.5% weight content. The ABS intake mechanism without graphite was adhesive. Microscope observations revealed that graphite introduction formed a third phase, improving tribological properties [27].

Studies by Gheisari et al. showed that graphite's physical form determines the composite surface topography after abrasion tests. Graphite flakes in polytetrafluoroethylene composite were 5-6 times larger than particles in polyimide

composite. Flakes mixed with PTFE caused non-uniform wear and uneven topography due to their larger size and stronger matrix bond [28]. Shang et al. studied polyether ether ketone (PEEK) composites with graphite particles, examining effects of graphite content and particle size on properties. Adding graphite decreased coefficient of friction, reaching minimum at 25 wt.%. PEEK/graphite composites showed higher wear rate due to graphite's layered structure. Smaller graphite particles improved wear resistance and mechanical properties by enhancing interfacial connection [29].

Suresha et al. studied graphite particles' effects on glass and carbon fibre laminates. Studies show glass fiber composite's tensile strength increases with graphite content. Graphite surface layer improved wear characteristics. Carbon-epoxy composite wear occurred through microcracks, but graphite filler reduced this by promoting layer transfer mechanisms [30, 31].

Studies by Bokarev et al. [32] and Matsumoto [33] highlighted the efficacy of inorganic nanoparticles and oxidised nanocarbons as additives to improve tribological properties of lubricants and epoxy resins, respectively. Addition of these nanomaterials increases hardness and lubricity, resulting in improved tribological performance of composite materials. Similarly, Chandrabhan et al. [34] and Yan et al. [35] investigated use of graphene oxide nanosheets and phosphorus-nitrogen additives to improve tribological properties by providing self-lubrication and active elements to reduce friction and wear rates. In addition, in research conducted by Ranjan et al. [36] and Liu et al. [37] project investigated use of $\text{TiO}_2/\text{gC}_3\text{N}_4$ nanoadditives and epoxy resins to enhance the oxidative properties of vegetable oils and improve underwater tribological properties, respectively. These additives interact with lubricant and form protective films that improve tribological performance.

The objective of this study is to examine the influence of graphite morphology on water absorption and fatigue properties of biopolyamide matrix composites. Incorporation of graphite into biopolyamide, either as flakes or expanded graphite, through surface and structural modifications, significantly reduces water absorption and enhances certain fatigue properties of the material. These effects, contingent upon the graphite structure, arise from variations in microstructure, stress distribution, and surface characteristics, rather than solely from well-documented

tribological properties of graphite. Previous research on polymer composites with graphite additives has predominantly focused on its impact on tribological properties, such as reduction of friction coefficient and material wear. This study extends existing knowledge by demonstrating that the morphology of graphite (flake versus expanded) is also critical for moisture absorption, fatigue properties, and resistance to thermal aging, areas that have been insufficiently explored in the context of biopolyamides. Analysis of material properties from different perspectives is extremely important because it allows for a better understanding of the mechanisms occurring in structure of composites during loads, especially dynamic loads. In the case of the materials studied – epoxy composites with silicon carbide microparticles – it was shown that their high heterogeneity at different structural scales significantly affects their physical and mechanical properties [38]. Research on composite materials, particularly those derived from biorenewable raw materials, is of significant importance in light of rapidly evolving technological trends and increasing environmental demands. Current developments in composite materials reveal a heightened interest in carbon fibre-reinforced thermoplastic polymer composites (CFRTPs), which are progressively being adopted in applications where traditional thermosetting resins once prevailed.

Carbon fiber-reinforced PA6 and PA12 polyamide composites are being developed for aerospace applications, offering cost-effectiveness and ease of processing for non-critical components like cable ducts and interior elements. These materials operate at temperatures from 80 °C to 130 °C and can be formed at high temperatures and reprocessed, making them ideal for complex aerospace shapes [39].

MATERIALS AND METHODS

Materials

In the experimental phase of the study, three materials were synthesized. Biopolyamide Eco-PaXX® Q150-D PA410 (DSM Plastic, Heerlen, Netherlands) served as the matrix. Two types of graphite were utilized as additives: graphite flakes with a size of 4 µm, exhibiting a distinct scale structure and a characteristic metallic luster. This material is employed as a component in sealing

materials, refractory products, and casting technology (FG 597, Grafity SINOGRAF, Toruń, Poland). Additionally, modified graphite, specifically expanding flake graphite, was used. Due to its expansion capabilities at elevated temperatures, it is also utilized as a flame retardant (antipyrène) in fire-resistant plastics or coatings (EG 290 Grafity SINOGRAF, Toruń, Poland). The graphite expansion temperature of 230 °C for 2h was employed. The test specimens were fabricated via injection molding using the processing parameters presented in Table 1. Prior to injection, the biopolyamide was subjected to drying for 24 hours at 80 °C. A description of the manufactured materials is presented in Table 2.

Methods of testing

DComposite densities was measured using hydrostatic method with a RADWAG WAS 22W laboratory scale (Radom, Poland). Water absorption was assessed using the gravimetric method in accordance with the PN-EN ISO 62:2008 standard [40]. Each time after the assumed period of incubation of the samples in water, the samples were dried with a paper towel and weighed. The weight was determined using an electronic Ohaus Adventurer laboratory balance (Parsippany, New Jersey, United States). Both static tension and static bending tests were conducted. For the impact testing, unnotched specimens were subjected to the Charpy method using a Zwick/Roell HIT5.5P hammer (Ulm, Germany) according to PN-EN ISO 179-1:2010 [41]. The static tensile test (PN-EN ISO 527-1:2010) [42] and static bending test (PN-EN ISO 178:2011)[43] were performed on a Shimadzu AGS-X 10 kN

testing machine (Kyoto, Japan) with a test speed of 10 mm/min. A series of strength tests were conducted utilizing digital image correlation (DIC) analysis. DIC method is a non-contact, image-based technique that processes digital images of deforming objects to calculate full-field displacements, deformations, and/or vibrations. This method provides more comprehensive data compared to traditional strain gauges and extensometers, offering both local and average information on deformation during mechanical testing. The GOM Aramis SRX system with GOM Corelate pro software was employed for DIC measurements. All strength tests were repeated after the accelerated thermal aging process using QUV accelerated weathering tester aging chamber (Q-LAB Corporation, Westlake, Ohio, USA). Method and parameters are described in detail in [44] according to the ASTM G154 standard [45]. The parameters of one cycle of the aging process are shown in Table 3, and this process was repeated for a period of 1000 hours.

The first mechanical hysteresis loops were devised to demonstrate the viscoelastic characteristics of the manufactured composites. The test involved an applied load of up to 60% of the maximum force required to break the sample, ascertained during the tensile test. This method sought to ascertain the displacement that arises during cyclic operation. The tests were conducted using a Shimadzu AGS-X 10 kN testing machine (Kyoto, Japan) equipped with software for energy dispersion analysis (Autograph Trapezium X). The loading and unloading speed were set at 10 mm/min.

Fatigue tests were conducted using an electrohydraulic servo fatigue testing machine,

Table 1. Injection molding parameters to produce testing specimens

Temperature (°C)							Injection pressure (bar)	Compression pressure (bar)	Press time (s)
Feed zone	Zone 1	Zone 2	Zone 3	Zone 4	Nozzle	Mold			
40	190	265	265	275	280	60	1200	600	8
Screw speed (RPM)		Back pressure (bar)		Injection speed (mm/s)			Gate design and location		
100		40		20			Edge gate		

Table 2. Description of manufactured materials

Index	Description
BioPA	100 % EcoPaXX® Q150-D PA410
10G	90% EcoPaXX® Q150-D PA410 +10wt. % graphite flakes FG 597
10GEXP	90% EcoPaXX® Q150-D PA410 +10wt. % expanded graphite EG 290

Table 3. Characteristics of the aging cycle

Cycle			
Function	Intensity (W/mw/nm)	Temperature (°C)	Time (min)
UV radiation	1.55	60	08:00
Shower	-	-	00:15
Condensation	-	50	03:45

specifically the Shimadzu EHF-E Series (Kyoto, Japan). The study was based on the principles of the Lehr method, originally developed for fatigue testing of metals as an alternative to the traditional Wohler method used for long-term testing [46]. The Lehr method is founded on the observation that a significant increase in energy dissipation, strain, and temperature of the tested samples typically occurs prior to fatigue failure. The core of this method involves assessing these parameters in an accelerated fatigue test, where cyclic loading increases in amplitude over time, and relating them to the maximum stress. This approach has proven effective in determining fatigue strength as a comparative parameter for evaluating the fatigue properties of polymer composites with a thermoplastic matrix [47]. Accelerated fatigue parameters encompassed an initial load of 5% of the material’s tensile strength (140 N), with a subsequent increase in amplitude of an additional 5% after 1000 cycles. The experiment was conducted until specimen failure occurred.

Tribological tests, including friction coefficient measurement, were carried out in accordance with the requirements of ISO 20808:2016 [48]. The T-01M tribotester developed by the Institute for Sustainable Technologies in Radom was used to carry out experiments. This device enables tribological studies of ball-target associations under conditions of sliding friction with the rotational motion of the sample.

A diagram of the tribological system is shown in Figure 1. This system consists of a disc in rotation (n) and a counter-sample in the form of a sphere, statically fixed and pressed against the surface of the disc with a preset normal force (P). The device is controlled by computer software, which enables ongoing data recording and determination of friction coefficient as a function of time or friction distance. The test parameters included measurement at two loads of 10 and 20 N. The friction distance was 250 m at a speed of 120 RPM.

To assess surface topography before and after the tests, a Profilm3D non-contact optical

profilometer from Filmetrics was used. It is an interference profilometer of white light enabling spatial representation of surface microgeometry in the form of three-dimensional digital models. The principle of operation of the device is based on the phenomenon of interference of light waves reflected from the tested object and the reference standard, which allows for precise roughness measurements.

RESULTS AND DISCUSSION

Mechanical investigation and water absorption

Water ingress into composite materials predominantly occurs through diffusion, wherein water molecules infiltrate the matrix and, to a lesser extent, the fibers. This process is influenced by factors such as the angle between the direction of water ingress and the orientation of the fibers. Additional pathways for moisture ingress include capillarity and migration through defined microcracks, which arise only after specific damage to the composites. Such

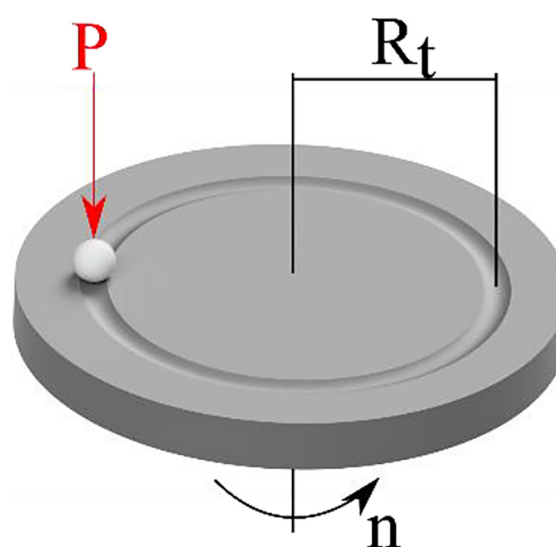


Figure 1. Diagram of the tribological system

damage, which facilitates moisture penetration by activating these supplementary pathways, often arises from the composite's exposure to moisture. Capillary mechanism involves the movement of water molecules along the fiber-matrix interface, followed by diffusion from this boundary into the polymer matrix. This mechanism is activated only if fiber-matrix separation has occurred, typically due to water-induced degradation at the interface. Moisture migration through microcracks encompasses both flow and retention of water within microcracks as well as other forms of micro-damage induced by environmental factors [49].

Figure 2 shows the results of the water absorption measurement. The study was conducted for 90 days. The results of the study show that introduction of graphite into polyamide causes a reduction in water absorption from 3.6% to 2.9%, which means that water absorption is reduced by 20%. This is a beneficial phenomenon because polyamides, as condensation polymers, absorb water up to 11%. In the case of biopolyamides, this effect has been reduced to about 4%, but the effect of moisture on the change in strength properties is quite significant, as it leads to plasticization of material. The reduction in water absorption by polyamide and other polymers after introduction of graphite powder or flakes is attributable to several related mechanisms, mainly due to the barrier properties and the modified microstructure of the composite. First of all, the lamellar morphology of graphite creates a tortuous path that water molecules must travel through to penetrate the polymer matrix [50, 51]. This structure forces the water to travel a longer and more

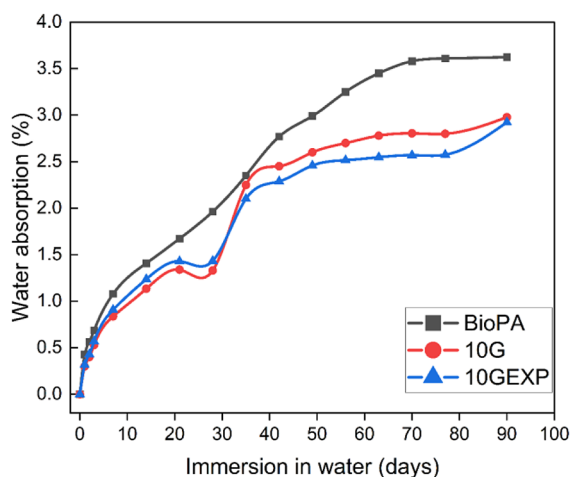


Figure 2. Water absorption of manufactured materials

complex route than pure polymer, which significantly reduces both the rate and the total amount of water absorbed.

In addition, graphite, as a hydrophobic material, hinders penetration of water into the composite, which translates into a further reduction in the rate of its absorption [51].

Equally essential is effective dispersion and sufficient interfacial bonding between graphite particles and the polymer matrix. This arrangement reduces the formation of microvoids and free spaces that would normally be water diffusion channels. Studies show that proper wetting of fillers by polymer resin increases the structural integrity of the composite, reducing its porosity and effectively “sealing” the material against moisture ingress [51, 52]. In the case of polyamides, the presence of such fillers reduces their hygroscopicity, which allows them to maintain dimensional stability and mechanical properties over a longer period of use. In addition, the reinforced interface limits the mobility of the polymer chains in the presence of moisture, reducing the plasticizing effect that water could have in the polymer network [53].

Another factor affecting barrier properties of composites is the orientation of the graphite particles during processing. When the flake particles are parallel to the surface of the material, they form a physical barrier that prevents water molecules from penetrating deeper. This type of layered structure proves to be particularly advantageous in applications that require both water resistance and high mechanical strength. Not only does it reduce water absorption, but it also increases the overall stability of the composite [51].

In conclusion, the combined effect of graphite's hydrophobicity, its favorable orientation in the structure, strengthened interfacial bonds, and the tortuous path effect provides a consistent explanation for observed reduction in water absorption in graphite-reinforced polymer composites, including polyamide-based systems [53].

The fundamental tests encompass determination of composite density and strength assessment to ascertain primary mechanical properties. The density of composites with graphite addition remained at a comparable level, measuring 1.104 ± 0.007 for polyamide, 1.145 ± 0.001 for the composite containing 10% graphite in flake form, and 1.150 ± 0.001 for the composite with 10% expanded graphite content. The results of the strength tests are presented in Figures 3–6.

The incorporation of graphite additives significantly reduced the material’s deformability and resistance to dynamic impacts. Biopolyamide exhibits a large deformation exceeding 50%, whereas the addition of graphite resulted in an approximately 10-fold decrease in deformation. The polyamide stretching curve reveals several distinct stages of deformation. Beyond the initial elastic phase and the onset of plastic deformation, there is a notable force drop, during which the sample undergoes significant constriction, leading to a reduction in recorded force. Subsequently, the material resumes plastic deformation until the test concludes with the sample fracturing. Notably, deformation is localized primarily within the constriction area. This phenomenon is characteristic of the behavior observed in the stretching of woven plastics, such as polyamides or polyethylene terephthalate. These findings were corroborated by the impact test (Figure 6). Furthermore, the introduction of graphite, particularly in its expanded form, causes a reduction in tensile strength. For the material modified with flake graphite, a slight reduction in tensile strength was observed. Other strength parameters increased, notably the modulus of elasticity for the material modified with graphite flakes.

To elucidate the mechanism by which graphite flakes enhance the Young’s modulus and flexural strength of polymer composites, it is instructive to analyze the findings of relevant studies. Research conducted by Ho et al. demonstrated that large graphite flakes are more efficacious in reinforcing epoxy composites compared to small

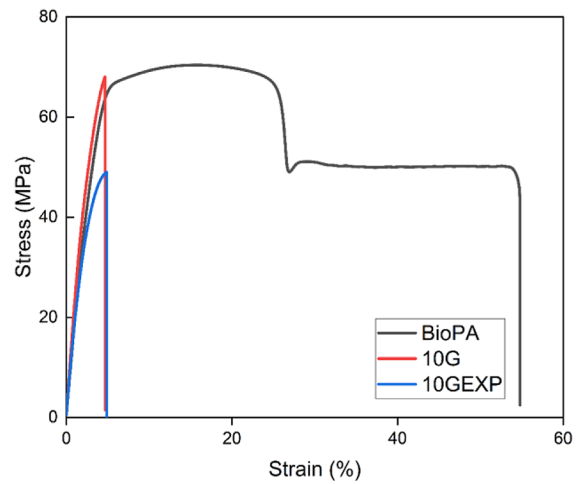


Figure 3. Example stress-strain curves for tested material

flakes, particularly with respect to flexural modulus [54]. Furthermore, Lim et al., in their investigation of polyamide composites (nylon 610), emphasize that the intact structure of graphite flakes and their interaction with the matrix material contributes to improved mechanical properties, including Young’s modulus and flexural strength. The authors underscore the significance of morphology and compatibility of graphite flakes within the composite matrix [55]. Ünal et al. conducted a study incorporating graphite fillers into composite materials with a polyamide-6 matrix, revealing variations in mechanical, electrical, and tribological properties based on differing percentages of graphite content, thereby highlighting the influence of graphite filler

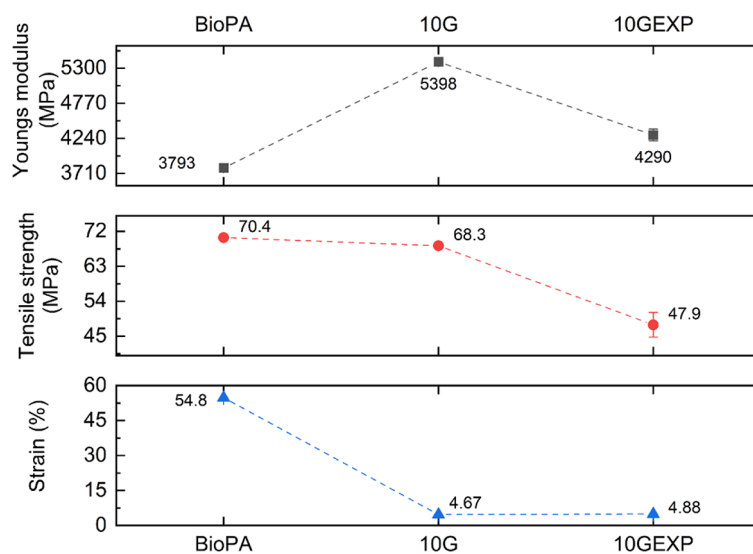


Figure 4. Comparison of the average strength values determined in the static tensile test

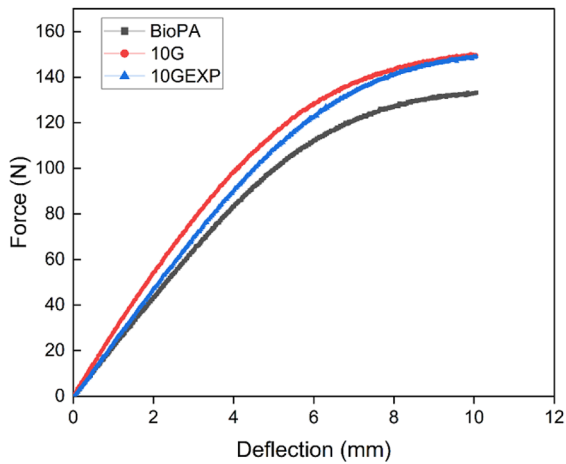


Figure 5. Example of bending curves for tested materials

concentration on the mechanical behavior of the composite [56]. Kalaitzidou et al. and Gaxiola et al. investigated polypropylene matrix composites and similarly demonstrate a positive effect of graphite flakes as reinforcement in polymer composites [57, 58]. The increase in Young’s modulus and flexural strength in polymer composites by graphite flakes involves several key factors that are substantiated in the literature. Primarily, the orientation of the graphite flakes in the composite matrix is essential. Studies by Zhou et al. and Banerjee et al. have demonstrated that graphite flakes align with their base planes perpendicular to the tensile direction, resulting in anisotropy of flexural strength and fracture toughness, thereby contributing to enhanced mechanical properties

[59, 60]. Furthermore, the morphology and structure of graphite flakes play a significant role in improving the mechanical properties of composites. Research by Lim et al. emphasizes that the intact structure of graphite flakes and their interaction with the matrix material are substantial reinforcement factors [55]. Moreover, Pandey et al. demonstrated that graphite flakes increase the thermal stability, thermal conductivity, and electrical conductivity of composites, indirectly influencing mechanical properties such as Young’s modulus and flexural strength [61]. Analyzing the properties of composites at various structural levels, encompassing both micro and macro scales and considering different loading modes such as shear, tension, and bending, is crucial. This comprehensive analysis facilitates a thorough understanding of the material’s performance under real-world operating conditions, identifies the key mechanisms responsible for the initiation and progression of damage, and optimizes the material design process to enhance resistance to cracking and other forms of degradation. Without such a multifaceted analysis, critical aspects of the material’s behavior may be overlooked, potentially leading to inaccurate assessments of its durability and safety in technical applications [38].

The produced materials were also subjected to tensile testing through the application of digital image correlation. Digital image correlation (DIC) is widely employed in the structural analysis of polymer composites. It is used to detect

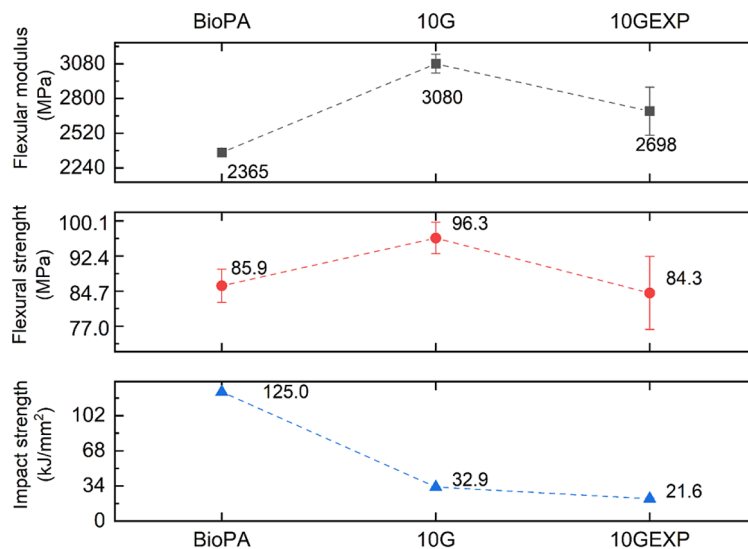


Figure 6. Comparison of the average values of strength properties determined at static bending and Charpy impact strength

delamination in polymer composites, thereby providing insights into internal structural damage [62, 63]. Aravind et al. investigated advancements in utilizing nanocrystalline cellulose for reinforcement of natural fibers in biocomposites, emphasizing progressions within this domain [64]. Moreover, digital image correlation was employed in the simulation of hybrid carbon-aramid composite materials, illustrating its effectiveness in the mechanical characterization and analysis of composite structures [65].

The sample images recorded using the digital image correlation technique illustrate areas where strain arises in the tested samples. Figure 7, obtained using the DIC technique, shows the strain distributions in the y-direction, corresponding to the direction of the tensile force. The results are presented using a color diagram on a vertical scale, reflecting the range from the minimum to the maximum strain values. In addition, the illustrations indicate the moments immediately preceding the fracture of the composites during the experiments. The areas showing the highest strain values in the y-direction are denoted by red areas along the measurement length. Numerous red areas are observed in the images, distributed inhomogeneously on the surface. The analysis of the obtained test results shows that the introduction of graphite in the form of powder causes a more uniform deformation along the entire length of the sample, while the unmodified material is characterized by a more nonuniform location of tensile stresses and strains. The introduction of expanded graphite causes the formation of weakened areas of the sample, where the largest local deformations occur, suggesting a non-uniform bulk structure of

the material. The images shown in Figure 7 were recorded at a strain rate of 1 mm/min.

Mechanical hysteresis loops and accelerated fatigue

Energy dissipation in low cyclic loaded

The tested materials were subjected to low-cycle loads. Tests of this nature are crucial for initially assessing the adhesion between the components of the composite. The initial hysteresis loops enable the determination of the energy dissipated in the system during cyclic loading. Energy in the material is dissipated through various mechanisms. In polymer material, it primarily occurs through internal friction between polymer chains. In composite materials, this additional energy is dissipated to alleviate stresses arising from production and those that occur between the composite components. After a defined stress threshold is overcome, additional energy is absorbed to separate components from each other and overcome frictional forces between the reinforcement and the matrix [66, 67].

Figure 8 illustrates the first and twentieth hysteresis loops recorded at 60% of the maximum force required to fracture the sample. The presented loops demonstrate a more pronounced effect of the addition of graphite in the form of flakes compared to expanded graphite. The introduced additives reduce the dynamic creep of polyamide. Figure 8b depicts differences in dissipation energy between the first and twentieth hysteresis loops. The base material and the composite with the addition of exposed graphite exhibited similar energy values both at the commencement and

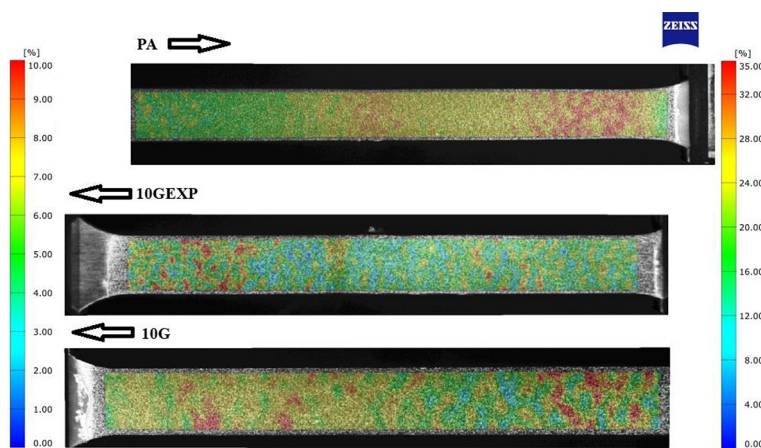


Figure 7. Sample images recorded utilizing the digital image correlation (DIC)

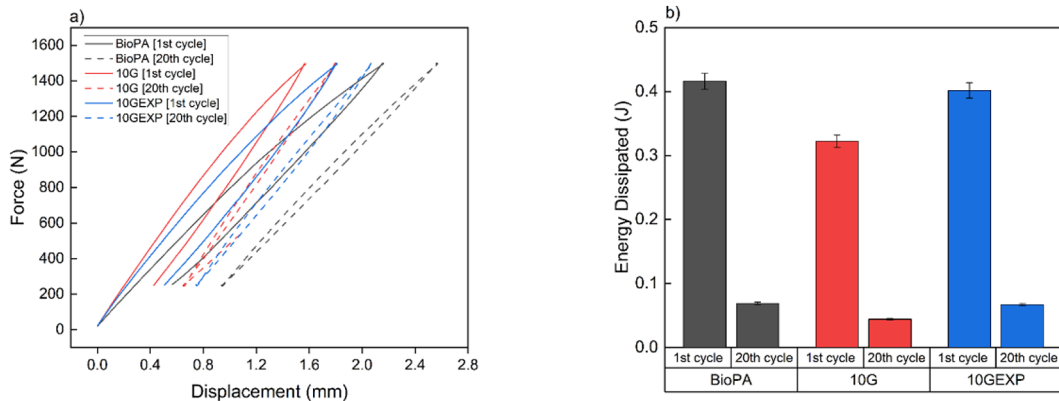


Figure 8. The first and twentieth hysteresis loops a) and energy dissipation b) determined for the molded composites

conclusion of the test, whereas the addition of flake graphite resulted in a reduction in the dissipation energy during the initial loading cycle relative to the base material. This observation, in relation to the aforementioned theory, may indicate a relatively strong interaction between composite components. Comparable research findings were reported for composites based on polyoxymethylene matrix [68, 69], polyamide [10–11], or thermoplastic elastomer [70]. The energy dissipated in polymer composites during the initial hysteresis loops is essential for comprehending the material’s behavior under cyclic loading. Furthermore, the initial hysteresis loops are utilized to characterize the viscoelastic nature of polymers. An example is the study of Panin et al., who examined the variability of the mechanical hysteresis loop in polyimide-CF-PTFE composites to evaluate low- and high-cycle fatigue. They emphasized the significance of the hysteresis loop region as a measure of energy loss and attenuation capacity during cyclic loading [71]. Dong et al. observed that the dissipated energy, represented by the hysteresis loop region, increased in the first compression cycle of carbon nanotube-reinforced double-lattice hydrogels (CNTs), indicating enhanced energy dissipation after the addition of CNTs [72]. Furthermore, Webber et al. noted substantial hysteresis during the first loading cycle of the dual-lattice hard hydrogels, which intensified with the maximum strain applied, underscoring the role of the initial hysteresis loop in energy dissipation [73]. Additionally, Krasnobrizha et al. elucidated the relationship between damage propagation, energy dissipation, and the manifestation of hysteresis loops in woven composites, emphasizing the

importance of understanding hysteresis behavior in relation to material damage [74].

Accelerated fatigue

Graphite-modified biopolyamide composites were subjected to accelerated fatigue tests with force excitation utilizing a sinusoidal profile. The tests were conducted in the loading-unloading mode, with a frequency of 5 Hz, on a hydraulic testing machine. For all composites, the value of the minimum excitation force remained constant throughout the test at 0.14 kN. The maximum load value in the initial 1000 test cycles was 0.28 kN. Subsequently, every 1.000 cycles, the maximum load level was increased by 0.14 kN (5% of the maximum force required to fracture the sample). Tests were conducted until sample failure occurred. Mechanical hysteresis loops were recorded, along with the maximum elongation and maximum value of dissipation energy obtained at each load level. Based on these data, fatigue strength was determined according to Lehr’s method as a comparative parameter for composites tested under identical conditions. Additionally, the relative fatigue strength was calculated by dividing the Lehr fatigue strength value by the tensile strength value of the composite.

The results of measurements from accelerated fatigue tests are presented in Table 4 and Figure 9–11. The maximum fatigue stress (σ_z), average elongation, and energy released in each range of the assumed load at the thousandth cycle or at the full cycle immediately preceding fracture were determined. The maximum cyclic loads carried corresponding to the maximally selected load for the test specimens were 69.6% for BioPA, 76.8% for 10G, and 87.7% for 10GEXP

of their maximum tensile forces. The base material, polyamide, exhibited a notably high elongation of the sample (19.8 mm) and the highest energy dissipation in the final order cycles. This phenomenon may be attributed to the heating of the viscoelastic matrix during cyclic loading and the increase in dynamic creep of the material. The recorded hysteresis loops shown in Figures 8–10 are characterized by an increase in surface area with an increasing number of cycles. The introduction of graphite particles enhances fatigue strength and significantly reduces dynamic creep. The most effective material was determined to be polyamide modified with graphite in the form of flakes, as it did not significantly reduce the tensile strength, resulted in an increase in the stiffness of the material, and demonstrated the highest fatigue strength.

Energy dissipation in polymer composites during low-cycle loads is a critical factor that significantly influences the behavior and performance of the material under repeated loading conditions. Numerous studies have investigated the mechanisms of energy dissipation in polymer composites subjected to low-cycle loads. For instance, Luo conducted experiments on precast

composite walls under low-cyclic reverse loading, demonstrating how the hysteretic curve region reflects the deformation capacity, energy dissipation capacity, and plasticity of the samples under such loading conditions [75]. Furthermore, Connesson et al. analyzed the evolution of the microstructure of a material under cyclic loading, examining the dissipation of energy due to internal friction, elucidating the relationship between microstructural changes and energy dissipation [76]. Additionally, Scott-Emuakpor et al. investigated the conservation of strain energy throughout the fatigue process, indicating that not all energy dissipated during cyclic loading contributes to the fatigue initiation process. These examples illustrate the complex nature of energy dissipation mechanisms in materials under cyclic loading conditions [77].

Cadavid et al. observed that the energy dissipated in the cycle at the conclusion of the fatigue period tends to increase due to the expansion of the area encompassed by the hysteresis loops [78]. Risitano et al. emphasized the significance of thermal analysis in evaluating the uniaxial fatigue strength of materials and mechanical components. They elucidated the role of temperature

Table 4. The level of maximum forces in hysteresis loops versus the increasing number of cycles and results of calculations: maximum stress at fatigue (Zz), tensile strength (σ_M), relative fatigue strength (relative to fatigue strength $Zz / \sigma_M \cdot 100\%$), mean elongation, energy dissipated in each cycle for tested composites

Samples	Maximum Force (kN)		Number of cycle			Zz, MPa			σ_M , MPa			Zz/ σ_M · 100 %		
	1	2	3	4	5	6	7	8	9	10	11	12	13	14
BioPA	1.96		12,840			24.5			70.4			34.80		
10G	2.1		13,780			31.2			68.3			45.68		
10GEXP	1.68		10,770			22.4			47.9			46.76		
The chosen level of Pmax, kN	0.28	0.42	0.56	0.70	0.84	0.98	1.12	1.26	1.40	1.54	1.68	1.82	1.96	2.1
Number of cycles, (*10 ³)	1	2	3	4	5	6	7	8	9	10	11	12	13	14
BioPA														
Mean elongation, mm	0.31	0.48	0.66	0.82	1.01	1.19	1.40	1.63	1.89	2.21	2.80	5.48	19.82*	-
Energy dissipated in each cycle	0.0003	0.0014	0.0034	0.0061	0.0103	0.0153	0.0230	0.0348	0.0499	0.0760	0.1389	0.3961	0.4566	-
10G														
Mean elongation, mm	0.28	0.42	0.56	0.70	0.83	0.97	1.11	1.25	1.39	1.53	1.67	1.80	1.88	4.90*
Energy dissipated in each cycle	0.0002	0.0008	0.0017	0.0034	0.0062	0.0099	0.0154	0.0230	0.0342	0.0533	0.0828	0.1330	0.3112	0.5566
10GEXP														
Mean elongation, mm	0.28	0.42	0.56	0.69	0.83	0.97	1.11	1.25	1.38	1.62	4.74*	-	-	-
Energy dissipated in each cycle	0.0003	0.0016	0.0043	0.0082	0.0137	0.0223	0.0343	0.0512	0.0759	0.1215	0.2076	-	-	-

Note: *Breaking the sample.

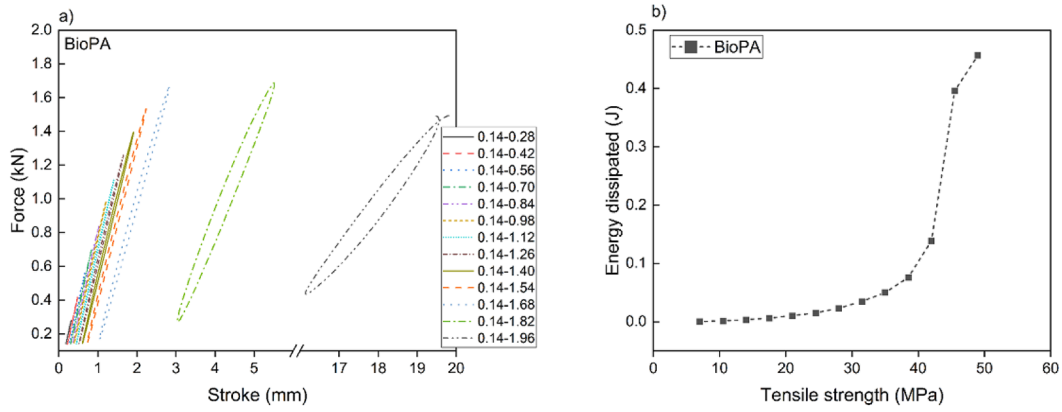


Figure 9. Accelerated fatigue results for biopolyamide: a) Recorded hysteresis loop, b) ratio of dissipation energy to applied stress level

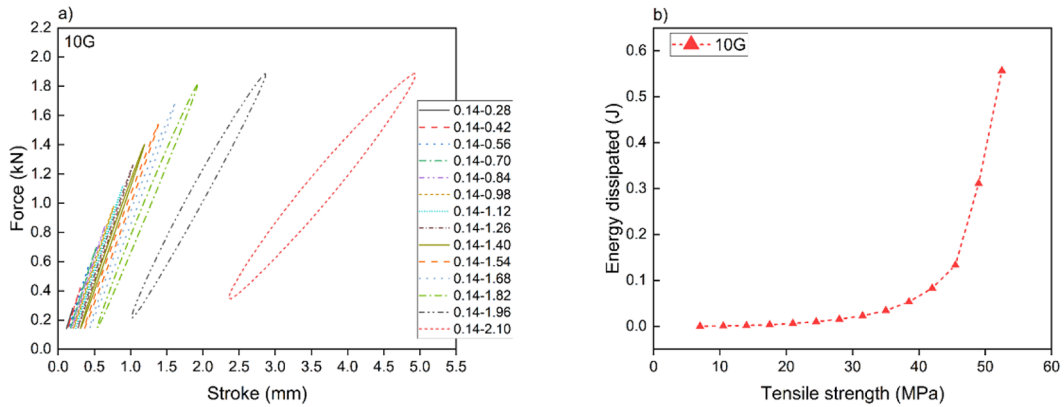


Figure 10. Accelerated fatigue results for biopolyamide with 10 wt.% of graphite flakes: a) recorded hysteresis loop, b) ratio of dissipation energy to applied stress level

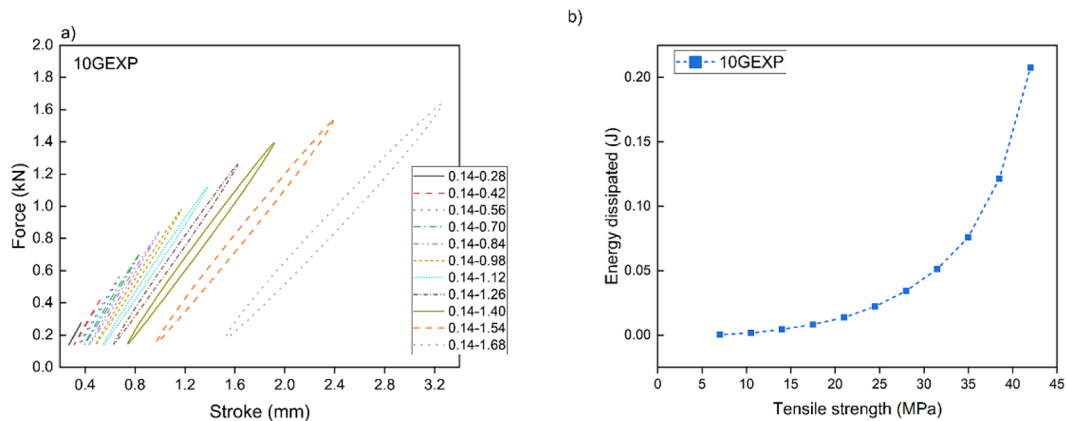


Figure 11. Accelerated fatigue results for biopolyamide with 10 wt.% of expanded graphite: a) recorded hysteresis loop, b) ratio of dissipation energy to applied stress level

in the energy process associated with fatigue-induced plastic energy [79]. The incorporation of graphite flakes into polyamide appears to result in increased fatigue-induced temperature dissipation, which consequently reduces dynamic creep

and facilitates increased dimensional stability of the samples. Comparable conclusions were drawn by Marat-Mendes et al. [80]. They identified the strengthening properties of graphite, as well as the enhanced thermal resistance, which

contributed to the overall mechanical performance of the composite, enabling more efficient energy dissipation during fatigue loading. This phenomenon is particularly significant in applications where materials are subjected to cyclic stress, as it contributes to delaying the onset of fatigue failure.

Furthermore, Khammassi and Tarfaoui emphasize the significance of graphite morphology, including its size and dispersion within the polymer. They assert that these factors play a crucial role in determining the mechanical performance of the resulting composite [81]. Additionally, properly dispersed graphite can function as a barrier to crack propagation, thereby enhancing the fatigue life of the material [82].

Aging investigation

Polymer aging can manifest in various forms, affecting their properties and shelf life over time. Scientific studies have identified different types of aging mechanisms, which include thermal aging [83], mechanical degradation, mechanochemical degradation [84, 85], chemical degradation [86]. Moisture absorption alone can contribute to changes in the strength characteristics of polymer composites, accelerating their aging under the influence of environmental factors [87]. The combination of multiple factors such as the effects of the aqueous environment, temperature or UV radiation results in a significant loss of almost all polymer properties, and understanding the effects of different types of polymer aging is essential to predict and manage the degradation

of polymer materials over time, thus ensuring their long-term performance and durability. On the basis of the literature indicated, it is possible to indicate possible changes and processes occurring in the structure of polymers and polymer composites, which are shown in Figure 12. The research examples presented by Sadritdinov et al. demonstrated a significant effect on moisture absorption, which contributes to changes in the strength characteristics of the composite, accelerating its aging under the influence of environmental factors [88]. Tue and Thwe discussed the strength behavior of the composite after aging, highlighting the critical role of interfacial adhesion between the fiber and the matrix polymer in maintaining mechanical properties over time [89]. This underscores the importance of considering the impact of aging on the durability and performance of polymer composites.

Figures 13–15 present the results of tests from the static tensile test for the fabricated materials both before and after the accelerated thermal aging process. The results demonstrated that the incorporation of graphite additives to biopolyamide enhances the resistance of composites to external factors. The impact of aging factors on biopolyamide resulted in a significant decrease in strength properties. Tensile strength decreased from 70 MPa to 25 MPa, modulus of elasticity by approximately 1 GPa, and strain at break reduced from over 50% to slightly above 1%. Materials modified with graphite particles also exhibited a decrease in strength properties; however, this decrease was within 10 MPa, considering tensile strength and a decrease in elastic

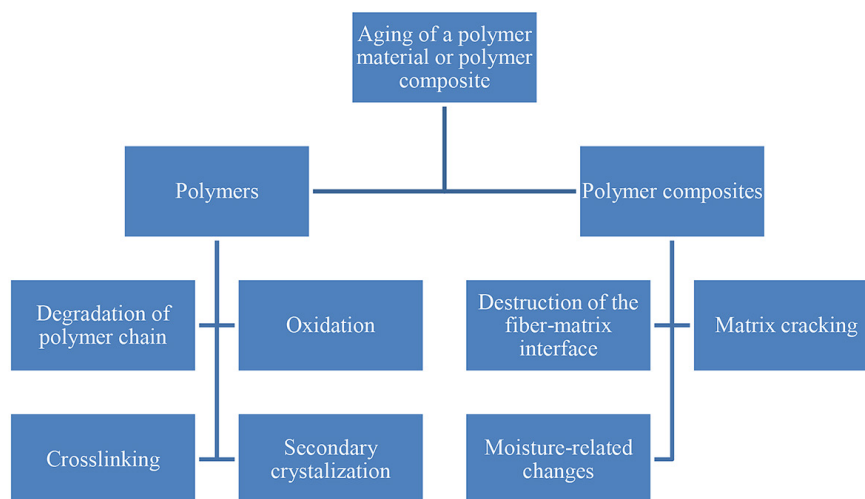


Figure 12. Changes in the structure of polymers and polymer composites due to material aging

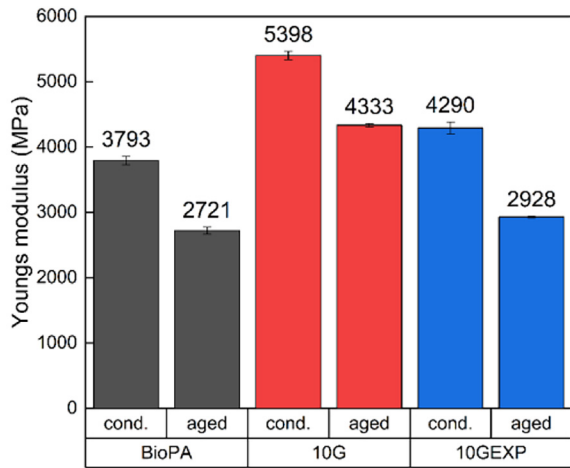


Figure 13. Youngs modulus before and after accelerated aging

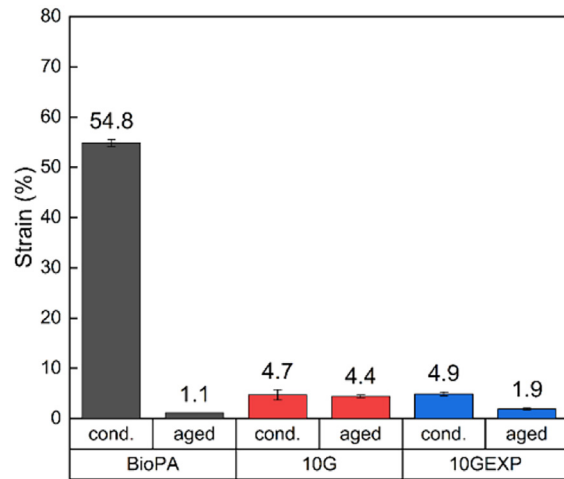


Figure 15. Strain at break before and after accelerated aging

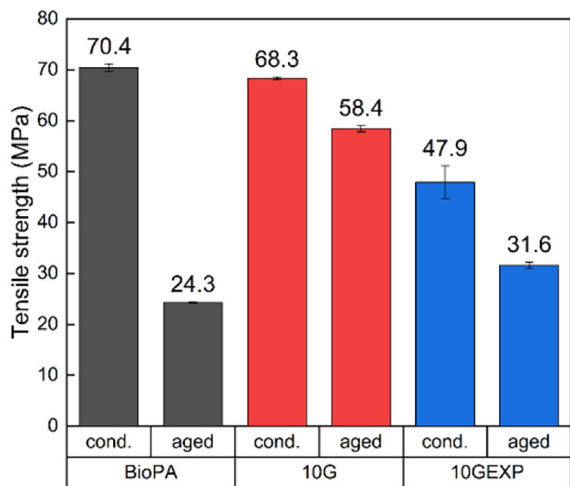


Figure 14. Tensile strength before and after accelerated aging

modulus at a similar level of approximately 1 GPa. No substantial changes were observed in deformation at break for the tested materials before and after the accelerated thermal aging process. The study results indicate that the incorporation of graphite into a biopolyamide matrix enhances resistance to aging factors.

Similar conclusions were reached by Zhao et al. These investigations demonstrated that graphite additives can enhance the thermal stability and tribological properties of polymers under conditions of elevated temperature and external environment [90]. Consequently, the findings of this study corroborate the hypothesis that graphite can mitigate the effects of high temperature on polymers, rendering it a

promising additive for improving the performance of polymer materials under harsh environmental conditions. One of the primary mechanisms by which graphite stabilizes polymers is through its exceptional thermal stability. Graphite, particularly in the form of exfoliated graphite, exhibits remarkable resistance to thermal degradation, which can significantly enhance the thermal stability of the polymer composite. For instance, research has demonstrated that the incorporation of graphite into polymers, such as polypropylene, results in increased thermal degradation temperatures, thereby providing a barrier against the thermal stresses that can lead to aging and degradation of the polymer matrix. The lamellar structure of graphite not only contributes to its thermal stability but also functions as a barrier to the diffusion of volatile degradation products, further protecting the polymer from aging effects [91].

Furthermore, graphite's capacity to absorb thermal energy contributes to the stabilization of the polymer matrix. The distinctive structure of graphite facilitates effective heat dissipation, which proves advantageous during thermal cycling conditions frequently encountered by polymers in service. This thermal absorption property mitigates the probability of thermally induced chain scission and other degradation mechanisms that may compromise the polymer's integrity over time. By occupying free volume within the polymer matrix, graphite constrains the mobility of polymer chains, a crucial factor in maintaining the structural integrity of the material under thermal stress [92].

Tribological investigation

Friction is the phenomenon of resistance to motion that arises at the point of contact between two bodies. With regard to the state of motion, a distinction is made between static friction (at the beginning or end of motion) and kinetic friction (during motion), with static friction usually being greater. Friction is also divided into internal (occurring within one body) and external (between two bodies on their contact surface). Another division is physical dry friction (clean surfaces) and technical friction (presence of impurities, gases and products of chemical reactions). In dry friction, most of the energy (about 90%) dissipates in the form of heat. Polymers are valued for their good tribological properties: wear resistance, low weight and vibration damping, but their disadvantage is low thermal conductivity and high thermal expansion. The operation of friction pairs depends on the actual contact surface (RPS), which affects frictional force, heat generation and wear. RPS is influenced by geometric (roughness) and physical (material character) factors [93, 94].

Adhesion between bodies is explained by several theories (mechanical, adsorption, electrical, diffusion, chemical). The breaking of intermolecular bonds can occur superficially (adhesively) or deep within the material (cohesively). Friction is affected by load, sliding speed and temperature. As the load and speed increase, the nature of the contact changes (from elastic to plastic), and the coefficient of friction can increase or decrease. In the friction-speed coefficient curve, there is often a maximum – its position depends on the structure and temperature of the polymer. The surface condition and structure of the polymer (crystallinity, chain orientation) also strongly influence the tribological properties. During friction, changes in the structure of the surface layer occur, macromolecules are destroyed and free radicals are formed, which can enter into chemical reactions, affecting wear and surface properties. Understanding friction processes allows you to design polymers with the desired tribological properties. Optimisation of these properties is possible, m.in other things, through modifications to the material structure, surfactants and various processing methods [95].

The results of the tests on the determination of the friction coefficient and surface roughness are presented in Figures 16–17 and Table 5.

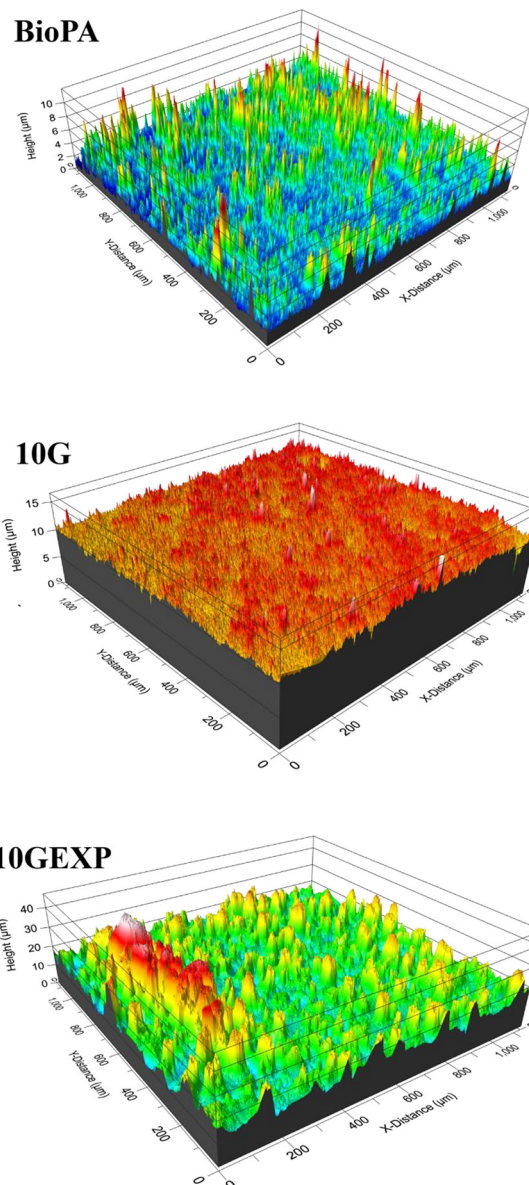


Figure 16. Surface topography of specimens

The coefficients of friction (CoF) obtained for the tested materials show clear differences depending on the type of filler used and the value of the normal force. Both BioPA and the composite with the addition of 10% graphite (10G) are characterized by low and stable CoF values, ranging from 0.072 to 0.081, with a slight decrease in the value when the load increases from 10 N to 20 N. A different characteristic is shown by the 10GEXP sample – at a load of 10 N it achieves a significantly higher coefficient of friction (0.212 ± 0.086), which, however, rapidly decreases to a level comparable to other materials (0.078 ± 0.002) at 20 N. This suggests that the sandwich structure of expanded graphite may require a

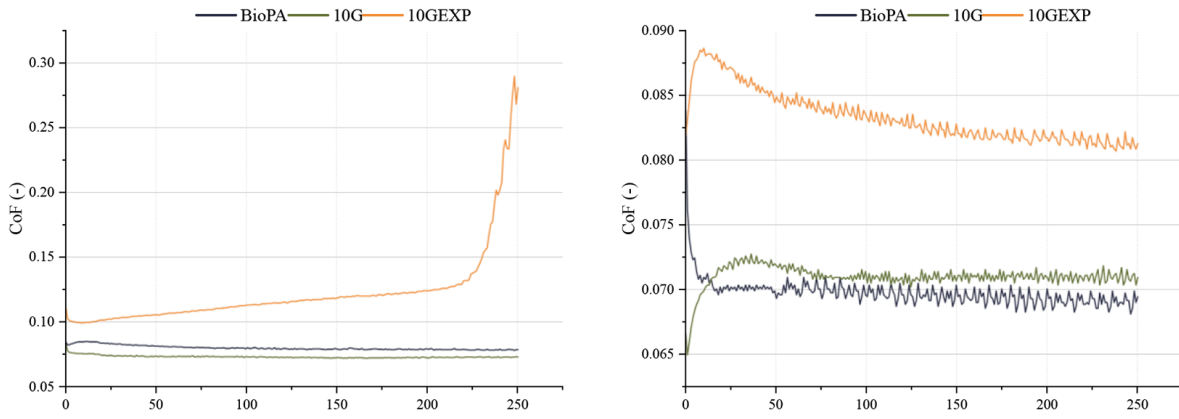


Figure 17. Results of tribological examinations

Table 5. Results of measurements of the friction coefficient and surface roughness

Material	10 N	20 N	Roughness Ra (μm)	Roughness Sa (μm)
	CoF (-)	CoF (-)		
BioPA	0.081 ± 0.001	0.074 ± 0.002	0.403	0.687
10G	0.077 ± 0.002	0.072 ± 0.001	0.266	0.425
10GEXP	0.212 ± 0.086	0.078 ± 0.002	0.996	2.933

sufficiently high pressure to activate the shear mechanism and generate a lubricating film.

The surface roughness parameters, described by the Ra and Sa indicators, show clear differences between the analyzed materials. The composite containing 10% graphite (10G) is characterized by the lowest roughness (Ra = 0.266 μm, Sa = 0.425 μm), while slightly higher values were obtained for pure BioPA (Ra = 0.403 μm, Sa = 0.687 μm). The highest roughness is shown by the sample with the addition of expanded graphite (10GEXP), for which the Ra and Sa values are 0.996 μm and 2.933 μm, respectively.

The relationship between roughness parameters and the coefficient of friction indicates that a more developed surface topography can contribute to an increase in frictional resistance, especially under low load conditions. The high roughness of 10GEXP correlates with the highest CoF value recorded at a load of 10 N (0.212 ± 0.086), which may be due to increased mechanical friction on a microscale, caused by the presence of numerous micropeaks and depressions affecting local contact conditions. At higher loads (20 N), when the graphite structures are effectively sheared and a lubricating film is formed, the roughness differences are

blurred, which is reflected in similar CoF values for all samples.

The influence of uneven microstructure in polymer composites containing expanded graphite on the coefficient of friction is a multifaceted phenomenon, significantly influenced by the quality of dispersion, particle flaking, and the formation of lubricating films at the sliding contact. When graphite is evenly dispersed, its internal layered structure can be effectively utilized, allowing the layers to slide and thereby reduce friction [96, 97]. Conversely, in instances of uneven dispersion or agglomeration, these advantages are mitigated by local stress concentrations and disruptions in transfer film formation. Research indicates that techniques such as exfoliation, sonication, or high-shear mixing can decrease the particle size of expanded graphite and enhance microstructural homogeneity [98]. This facilitates the consistent formation of a continuous lubricating film, which is essential for stable frictional behavior. An uneven distribution of the filler results in the formation of clusters, which interfere with the uniform deformation of the contact surface and the effective formation of the transfer film, potentially causing fluctuations or an increase in the coefficient of friction [99]. In polymer composites, the interfacial

bond between the matrix and the graphite is also critical. The uneven distribution of graphite affects the variable density of hydrogen bonds, thereby altering the tribological response [99]. Furthermore, microstructural heterogeneity can lead to local variations in mechanical and thermal reactions during slippage, destabilizing lubrication mechanisms [97, 100]. In conclusion, although expanded graphite inherently reduces friction when homogeneously integrated into the matrix, microstructural irregularities can negate these benefits. Therefore, optimizing processing methods to ensure uniformity is imperative. The balance between the properties of well-exfoliated layers and the effects of agglomeration ultimately determines the tribological behavior of the composite.

Lower roughness values for BioPA and 10G promote the stabilization of the coefficient of friction regardless of the normal force. It can be assumed that a more homogeneous surface reduces local increases in contact stress and facilitates the formation of regular sliding zones. Thus, the surface topography is an important factor determining the friction conditions, affecting the initial pressure distribution, the number of active microcontacts and the efficiency of the autolubrication mechanisms present in graphite-filled composites.

Shang et al. found that PEEK/graphite composites exhibited optimal tribological behaviour when the graphite content was 25 wt% [101]. In addition, Li et al. found that the tribological properties of glass fibre reinforced polyamide 6 composites were significantly improved by using graphite together with PTFE and UHMWPE [102]. Alajmi and Shalwan emphasized that graphite as an additive to polymer composites has a positive effect on tribological properties [103]. Moreover, Katiyar et al. showed that the addition of graphene oxide, graphite, and carbon nanotubes to polymers improved tribological properties [104]. This finding is consistent with a study by Sakka et al., which showed that treated carbon nanotubes/epoxy composites showed better tribological behavior [105]. Additionally, Przekop et al. (2020) highlighted that graphite effectively improves the tribological properties of polymer materials [106].

To determine which form of graphite – graphite flakes, graphite powder or expanded graphite – provides better tribological properties in polymer composites, several studies provide valuable

insights. Feng et al. found that graphite flakes in polypropylene composites form a continuous thermally conductive network, indicating their potential to increase thermal conductivity [107]. Guo and Yang mentioned that expanded graphite, along with other forms of graphite, has been used to improve the wear resistance of copper-based composites, suggesting its positive effects on tribological properties [108]. In addition, Jin et al. investigated the comparative tribological behaviour of resin-based friction materials containing natural graphite and expanded graphite, highlighting the importance of the type of graphite in influencing tribological performance [109]. Li et al. (2013) highlighted the importance of graphite as a solid lubricant in friction mitigation in polymer composites, pointing to its positive effect on tribological behavior [102]. Katiyar et al. discussed the importance of graphite powder as a filling material for improving tribological properties in various matrices [110]. Collectively, these studies indicate that various forms of graphite significantly contribute to enhancing the tribological properties of polymer composites. In summary, based on the synthesis of the referenced studies, it can be inferred that graphite flakes, graphite powder, and expanded graphite possess the potential to enhance the tribological characteristics of polymer composites. The selection of the most appropriate form of graphite may be contingent upon the specific requirements for composites and the processing conditions.

Microscopic observations

Figures 18–20 illustrate the microstructure of the materials under investigation. Figure 18 depicts the structure of the base materials. Polyamide is characterized by a relatively plastic fracture, as corroborated by strength tests, which indicate a deformation at break of approximately 50%. The incorporation of graphite, both in the form of powder and expanded graphite flakes, alters the fracture behavior from ductile to brittle. Microscopic images reveal a more intricate structure with sharp edges, indicative of the brittle nature of the fracture. Figure 18, which presents the structure of a composite modified with graphite flakes, highlights the distinctive features of expanded graphite (Figure 20), consisting of parallel graphite planes.

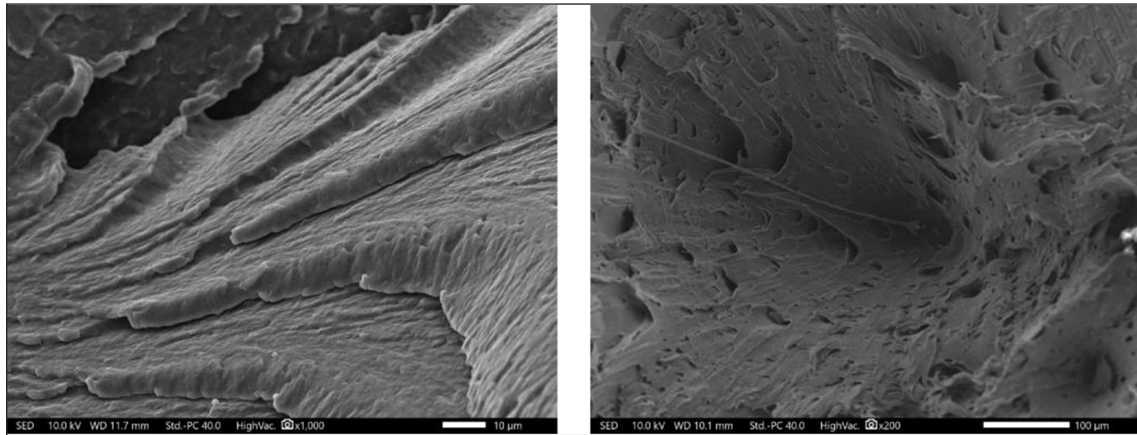


Figure 18. Microstructure of biopolyamide

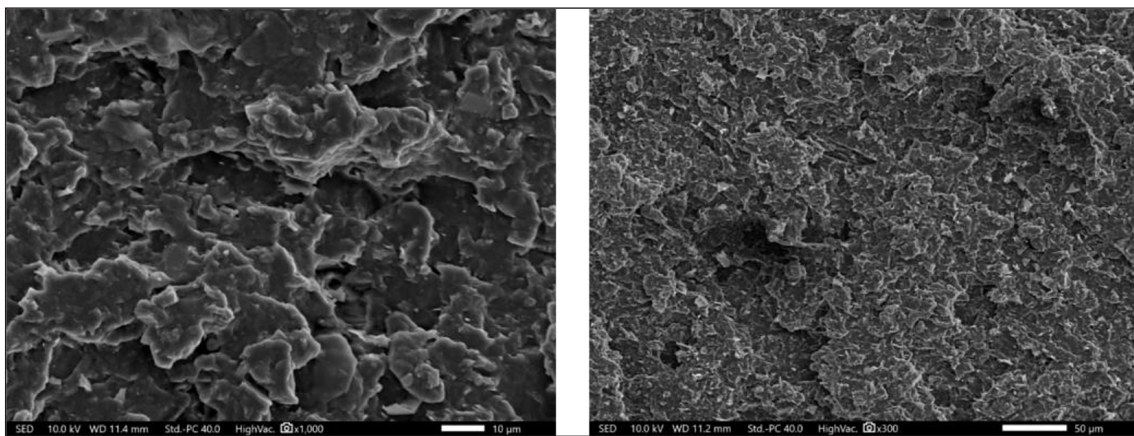


Figure 19. Microstructure of the composite with the addition of 10% wt. graphite in flakes

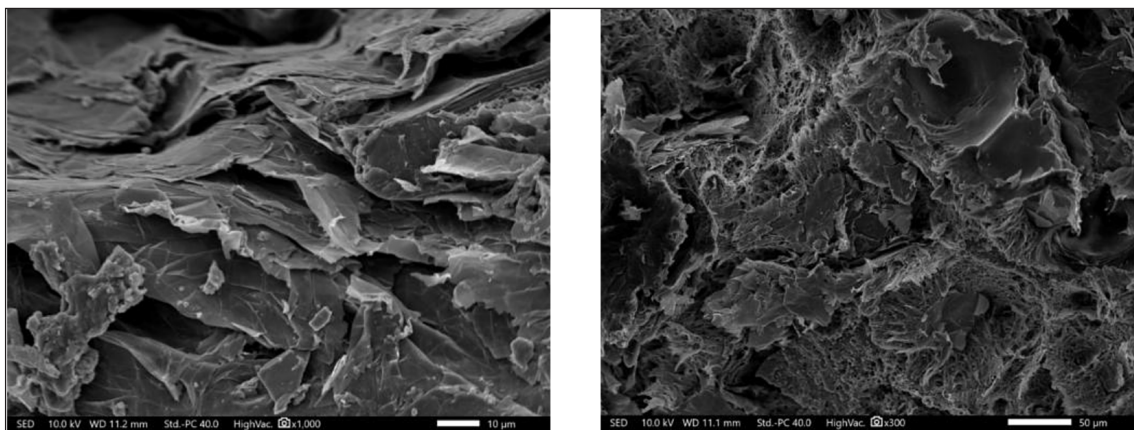


Figure 20. Microstructure of the composite with the addition of 10% wt. expanded graphite

CONCLUSIONS

The research conducted elucidates the impact of graphite morphology on the properties of biopolyamide-based composites, with a particular focus on water absorption, fatigue behavior, and

mechanical and tribological properties. The incorporation of graphite, in both flake and expanded forms, resulted in a 20% reduction in water absorption. This phenomenon is attributed to the formation of a tortuous path within the material structure, facilitated by the lamellar morphology

of graphite, the hydrophobic nature of the filler, and enhanced interfacial adhesion between the filler and the polymer matrix. The composites demonstrated a significant reduction in dynamic creep and a notable improvement in fatigue resistance, especially in the material modified with flake graphite, where the increase in fatigue strength reached 30% compared to the base material. The addition of flake graphite led to a 40% increase in the modulus of elasticity, whereas expanded graphite resulted in a 10% increase. Concurrently, a decrease in tensile strength was observed – by a few percent for composites with flake graphite and by 30% for those with expanded graphite. The study further confirmed that the selected graphite morphology effectively mitigates the adverse effects of thermal aging. Graphite-modified materials retained their key mechanical properties after accelerated thermal aging, with the decrease in the modulus of elasticity limited to 20% and in tensile strength to 15%, in contrast to unmodified biopolyamide, which exhibited decreases of 30% and 70%, respectively. Regarding tribological properties, expanded graphite significantly influenced the coefficient of friction under low-load conditions, increasing it to 0.212 at 10 N; however, under higher loads, all composites exhibited low, stable coefficient of friction values (approximately 0.078–0.081). It is also noteworthy that while the addition of graphite decreased the elongation at break and impact strength, it resulted in a substantial increase in stiffness and stable friction behavior. The results confirm that graphite-modified biopolyamides facilitate the design of composite materials with a balanced profile of mechanical, moisture resistance, and tribological performance. These findings open new avenues in materials engineering for the development of environmentally friendly, high-performance materials for technical applications.

Acknowledgements

This research was funded in whole or in part by National Science Centre, Poland, Grant number: DEC-2024/08/X/ST11/00531 (Biokompozyty na osnowie biopoliamidu o obniżonej absorpcji wody i zwiększonej wytrzymałości zmęczeniowej) as part of the MINIATURE 8 competition. For the purpose of Open Access, the author has applied a CC-BY public copyright licence to any Author Accepted Manuscript (AAM) version arising from this submission.

REFERENCES

1. Winnacker, M.; Rieger, B. Biobased Polyamides : Recent Advances in Basic and Applied Research. 2016, 1–23, doi:10.1002/marc.201600181.
2. Armioun, S.; Panthapulakkal, S.; Scheel, J.; Tjong, J.; Sain, M. Sustainable and Lightweight Biopolyamide Hybrid Composites for Greener Auto Parts. 2016, 9999, 1–9, doi:10.1002/cjce.22609.
3. Phanthuwongpakdee, J.; Babel, S.; Dwivedi, S.; Takada, K. Supporting Information For Anion-Scavenging Biopolyamides from Quaternized 4-Aminocinnamic Acid Photodimer. 1–8.
4. Ali, M.A.; Tateyama, S.; Oka, Y.; Kaneko, D.; Okajima, M.K.; Kaneko, T. Syntheses of high-performance biopolyamides derived from itaconic acid and their environmental corrosion. *Macromolecules* 2013, 46, 3719–3725, doi:10.1021/ma400395b.
5. Koziol, A.; Paso, K.G.; Kuciel, S. Properties and recyclability of abandoned fishing net-based plastic debris. *Catalysts* 2022, 12, 948, doi:10.3390/catal12090948.
6. gülel, ş.; güvenilir, y. preparation and characterization of novel bio-based polyamide 5.6 composites as sustainable alternatives to petroleum-derived polyamide 6.6. *Polym Compos* 2024, 45, 11033–11043, doi:10.1002/pc.28529.
7. Radzik, P.; Leszczyńska, A.; Pieliowski, K. Modern biopolyamide based materials: synthesis and modification. *Polymer Bulletin* 2019, doi:10.1007/s00289-019-02718-x.
8. Sagsoz, N.P.; Yanikoglu, N.; Ulu, H.; Bayındır, F. Color changes of polyamid and polymethyl methacrylate denture base materials. *Open J Stomatol* 2014, 4, 489–496, doi:10.4236/ojst.2014.410066.
9. Núñez Carrero, K.C.; Herrero, M.; Alonso, L.E.; Lizalde-Arroyo, F.; Salmazo, L.O.; Merino, J.C.; Rodríguez-Pérez, M.Á.; Barajas, J.M.P. Biopolyamide composites for fused filament manufacturing: impact of fibre type on the microstructure and mechanical performance of printed parts. *Progress in Additive Manufacturing* 2023, 9, 857–874, doi:10.1007/s40964-023-00486-9.
10. Romańska, P.; Kuciel, S. PA 10.10 and PA 6 composites with glass or basalt fiber: mechanical properties in dry and wet state. *Polimery/Polymers* 2024, 69, 159–166, doi:10.14314/polimery.2024.3.2.
11. Bazan, P.; Wierzbicka-Miernik, A.; Kuciel, S. A novel hybrid composites based on biopolyamide 10. 10 with basalt / aramid fibers : Mechanical and thermal investigation. 2021, 223, doi:10.1016/j.compositesb.2021.109125.
12. Bednarowski, D.; Bazan, P.; Kuciel, S. Enhancing strength and sustainability : evaluating glass and basalt fiber-reinforced biopolyamide as alternatives for. *Polymers (Basel)* 2023, 15, 3400.

13. Herrero, M.; Asensio, M.; Núñez, K.; Merino, J.C.; Pastor, J.M. Morphological, thermal, and mechanical behavior of polyamide11/sepiolite bio-nanocomposites prepared by melt compounding and in situ polymerization. *Polym Compos* 2019, 40, E704–E713, doi:10.1002/pc.24962.
14. Marset, D.; Dolza, C.; Boronat, T.; Montanes, N.; Balart, R.; Sanchez-Nacher, L.; Quiles-Carrillo, L. Injection-molded parts of partially biobased polyamide 610 and biobased halloysite nanotubes. *Polymers (Basel)* 2020, 12, 1–15, doi:10.3390/polym12071503.
15. Baniasadi, H.; Madani, Z.; Mohan, M.; Vaara, M.; Lipponen, S.; Vapaavuori, J.; Seppälä, J. V. Heat-induced actuator fibers: starch-containing biopolyamide composites for functional textiles. *ACS Appl Mater Interfaces* 2023, 15, 48584–48600, doi:10.1021/acsami.3c08774.
16. Basso, M.; Piselli, A.; Simonato, M.; Furlanetto, R.; Pupure, L.; Joffe, R.; De Nardo, L. Effect of food chemicals and temperature on mechanical reliability of bio-based glass fibers reinforced polyamide. *Compos B Eng* 2019, 157, 140–149, doi:10.1016/j.compositesb.2018.08.078.
17. Sergi, C.; Vitiello, L.; Russo, P.; Tirillò, J.; Sarasini, F. Toughened bio-polyamide 11 for impact-resistant intraply basalt/flax hybrid composites. *Macromol* 2022, 2, 154–167, doi:10.3390/macromol2020010.
18. Abdelbary, A. *Wear of Polymers and Composites*; Woodhead Publishing is an imprint of Elsevier: Cambridge, UK, 2016; 17.
19. Bazan, P.; Nykiel, M.; Kuciel, S. Influence of silicone oil on physico-mechanical and tribological properties of hybrid composites reinforced with basalt fiber/PTFE particles based on polyoxymethylene (POM). *Journal of Thermoplastic Composite Materials* 2023, 36, 141–161, doi:10.1177/0892705721989779.
20. Bazan, P.; Kuciel, S.; Nykiel, M. Characterization of composites based on polyoxymethylene and effect of silicone addition on mechanical and tribological behavior. *Polym Eng Sci* 2019, 59, 935–940, doi:10.1002/pen.25039.
21. Nawaz, S.; Khan, Y.; Khalid, S.; Malik, M.A.; Siddiq, M. Molybdenum disulfide (MoS₂) along with graphene nanoplatelets (GNPs) utilized to enhance the capacitance of conducting polymers (PANI and PPy). *RSC Adv* 2023, 13, 28785–28797, doi:10.1039/d3ra04153k.
22. Biryukov, V.; Yakubovsky, A. Tribotechnical Characteristics of Polyamide PA 6 with Additives of Molybdenum Disulfide and Graphite. *E3S Web of Conferences* 2023, 458, doi:10.1051/e3sconf/202345802018.
23. Marcus, H.L. *Molecular Characterisation of Composite Interfaces*; 1987; 91.
24. Stabik, J.; Dybowska, A. Electrical and tribological properties of gradient epoxy-graphite composites. *Journal of Achievements in Materials and Manufacturing Engineering* 2008, 27, 39–42.
25. Li, X.; Gao, Y.; Xing, J.; Wang, Y.; Fang, L. Wear reduction mechanism of graphite and MoS₂ in epoxy composites. *Wear* 2004, 257, 279–283, doi:10.1016/j.wear.2003.12.012.
26. Sathees Kumar, S.; Kanagaraj, G. Investigation on mechanical and tribological behaviors of PA6 and graphite-reinforced PA6 polymer composites. *Arab J Sci Eng* 2016, 41, 4347–4357, doi:10.1007/s13369-016-2126-2.
27. Ben Difallah, B.; Kharrat, M.; Dammak, M.; Monteil, G. Mechanical and tribological response of abs polymer matrix filled with graphite powder. *Mater Des* 2012, 34, 782–787, doi:10.1016/j.matdes.2011.07.001.
28. Gheisari, R.; Polycarpou, A.A. Tribological performance of graphite-filled polyimide and PTFE composites in oil-lubricated three-body abrasive conditions. *Wear* 2019, 436–437, 203044, doi:10.1016/j.wear.2019.203044.
29. Shang, Y.; Zhao, Y.; Liu, Y.; Zhu, Y.; Jiang, Z.; Zhang, H. The effect of micron-graphite particle size on the mechanical and tribological properties of PEEK composites. *High Perform Polym* 2018, 30, 153–160, doi:10.1177/0954008316685410.
30. Suresha, B.; Siddaramaiah; Kishore; Seetharamu, S.; Kumaran, P.S. Investigations on the influence of graphite filler on dry sliding wear and abrasive wear behaviour of carbon fabric reinforced epoxy composites. *Wear* 2009, 267, 1405–1414, doi:10.1016/j.wear.2009.01.026.
31. Suresha, B.; Chandramohan, G.; Renukappa, N.M. Mechanical and tribological properties of glass-epoxy composites with and without graphite particulate filler. *J Appl Polym Sci* 2007, 103, 2472–2480.
32. Bokarev, D.A.; Bakunin, V.N.; Kuz'mina, G.N.; Parenago, O.P. Highly Effective Friction Modifiers from Nano-Sized Materials. *Chemistry and Technology of Fuels and Oils* 2007, 43, 305–310, doi:10.1007/s10553-007-0054-2.
33. Matsumoto, N.; Yuki Yoshi, Y.; Omiya, Y.; Kinoshita, H. Improvement of tribological properties of epoxy resin by addition of oxidized nanocarbons. *Tribology Online* 2020, 15, 78–88, doi:10.2474/TROL.15.78.
34. Chandrabhan, S.R.; Jayan, V.; Parihar, S.S.; Ramaprabhu, S. Development of a nitrogen-doped 2D material for tribological applications in the boundary-lubrication regime. *Beilstein Journal of Nanotechnology* 2017, 8, 1476–1483, doi:10.3762/bjnano.8.147.
35. Yan, J.; Bai, X.; Li, J.; Ren, T.; Zhao, Y. The tribochemical study of novel phosphorous-nitrogen

- (P-N) type phosphoramidate additives in water. *Industrial Lubrication and Tribology* 2014, 66, 346–352, doi:10.1108/ilt-12-2011-0111.
36. Ranjan, N.; Shende, R.C.; Kamaraj, M.; Ramaprabhu, S. Utilization of TiO₂/GC₃N₄ nanoadditive to boost oxidative properties of vegetable oil for tribological application. *Friction* 2021, 9, 273–287, doi:10.1007/s40544-019-0336-9.
 37. Liu, Y.; Gao, G.; Jiang, D.; Yin, Z. Enhancement of underwater tribological properties of hybrid PTFE/nomex fabric laminate composites by epoxy resins. *ACS Omega* 2022, 7, 7737–7744, doi:10.1021/acsomega.1c06524.
 38. Stukhlyak, P.D.; Buketov, A. V.; Panin, S. V.; Maruschak, P.O.; Moroz, K.M.; Poltaranin, M.A.; Vukherer, T.; Kornienko, L.A.; Lyukshin, B.A. structural fracture scales in shock-loaded epoxy composites. *Physical Mesomechanics* 2015, 18, 58–74, doi:10.1134/S1029959915010075.
 39. Fantastic Thermoplastics Novel Techniques and Materials Are Accelerating a Rethink of Aerostructure Production. Available online: <https://www.airbus.com/en/newsroom/stories/2025-01-fantastic-thermoplastics> (accessed on 19 April 2025).
 40. INTERNATIONAL STANDARD ISO 62:2008. Plastics — Determination of Water Absorption;
 41. INTERNATIONAL STANDARD ISO 179-1:2010. Plastics — Determination of Charpy Impact Properties;
 42. INTERNATIONAL STANDARD ISO 527-1:2012. Plastics — Determination of Tensile Properties;
 43. INTERNATIONAL STANDARD ISO 178:2010. Plastics — Determination of Flexural Properties;
 44. Badura, K. Effect of nano and micro size of copper oxide on the properties of thermoplastic elastomer. *Advances in Science and Technology Research Journal* 2024, 18.
 45. American Standard for Measuring Accelerated Weather Testing ASTM G154. Standard Practice for Operating Fluorescent Ultraviolet (UV) Lamp Apparatus for Exposure of Materials;
 46. Vitovec, F.H.; Lazan, B.J. Strength, damping, and elasticity of materials under increasing reversed stress with reference to accelerated fatigue testing. *Proceedings of the American Society of Testing Materials* 1955, 55, 844.
 47. Liber-Kneć, A.; Kuźniar, P.; Kuciel, S. Accelerated fatigue testing of biodegradable composites with flax fibers. *J Polym Environ* 2015, 23, 400–406, doi:10.1007/s10924-015-0719-6.
 48. INTERNATIONAL STANDARD ISO 20808:2016. Fine Ceramics (Advanced Ceramics, Advanced Technical Ceramics) — Determination of Friction and Wear Characteristics of Monolithic Ceramics by Ball-on-Disc Method;
 49. Duncan, B.C.; Broughton, W.R. Measurement good practice guide No. 102 absorption and diffusion of moisture in polymeric materials. *Measurement Good Practice Guide* 2007.
 50. Phuangngamphan, M.; Okhawilai, M.; Hiziroglu, S.; Rimdusit, S. Development of highly conductive graphite-/graphene-filled polybenzoxazine composites for bipolar plates in fuel cells. *J Appl Polym Sci* 2019, 136, doi:10.1002/app.47183.
 51. Alo, O.A.; Otunniyi, I.O. Comparative study of flexural and physical properties of graphite-filled immiscible polypropylene/epoxy and high-density polyethylene/epoxy blends. *Polymers and Polymer Composites* 2021, 29, S1103–S1112, doi:10.1177/09673911211047027.
 52. Plengudomkit, R.; Okhawilai, M.; Rimdusit, S. Highly filled graphene-benzoxazine composites as bipolar plates in fuel cell applications. *Polym Compos* 2016, 37, 1715–1727, doi:10.1002/pc.23344.
 53. Perdum, A.-I.; Banu, A. The influence of water absorption on reinforced polymers (FRP) using MW-CNT and HGB. *Revue Roumaine de Chimie* 2023, 68, 101–107, doi:10.33224/rrech.2023.68.1-2.10.
 54. Ho, Q.B.; Osazuwa, O.; Modler, R.; Daymond, M.; Gallerneault, M.T.; Kontopoulou, M. Exfoliation of graphite and expanded graphite by melt compounding to prepare reinforced, thermally and electrically conducting polyamide composites. *Compos Sci Technol* 2019, 176, 111–120, doi:10.1016/j.compscitech.2019.03.024.
 55. Lim, J.V.; Bee, S.T.; Sin, L.T.; Ratnam, C.T.; Bee, S.L. Study of thermal effect on the mechanical properties of nylon 610 nanocomposites with graphite flakes that have undergone supercritical water treatment at different temperatures. *Polymers (Basel)* 2022, 14, doi:10.3390/polym14245494.
 56. Unal, H.; Esmer, K.; Mimaroglu, A. Mechanical, electrical and tribological properties of graphite filled polyamide-6 composite materials. *Journal of Polymer Engineering* 2013, 33, 351–355, doi:10.1515/polyeng-2013-0043.
 57. Kalaitzidou, K.; Fukushima, H.; Miyagawa, H.; Drzal, L.T. Flexural and tensile moduli of polypropylene nanocomposites and comparison of experimental data to Halpin-Tsai and Tandon-Weng Models. *Polym Eng Sci* 2007, 47, 1796–1803, doi:10.1002/pen.
 58. Gaxiola, D.; Jubinski, M.; Keith, J.; King, J.; Miskioğlu, I. Effects of carbon fillers on tensile and flexural properties in polypropylene-based resins. *J Appl Polym Sci* 2010, 118, 1620–1633, doi:10.1002/app.
 59. Zhou, S.; Wang, Z.; Zhang, W. Effect of graphite flake orientation on microstructure and mechanical properties of ZrB₂-SiC-graphite composite. *J Alloys Compd* 2009, 485, 181–185, doi:10.1016/j.jallcom.2009.05.126.

60. Banerjee, S.; Pattnayek, S.; Kumar, R.; Kar, K.K. Impact of graphite on thermomechanical, mechanical, thermal, electrical properties, and thermal conductivity of HDPE/copper composites. *Fuel Cells* 2020, 20, 116–130, doi:10.1002/fuce.201900004.
61. Pandey, A.K.; Singh, K.; Kar, K.K. Thermo-mechanical properties of graphite-reinforced high-density polyethylene composites and its structure–property corelationship. *J Compos Mater* 2017, 51, 1769–1782, doi:10.1177/0021998316683782.
62. Zhang, X.; Li, S.; Li, J.; Fu, B.; Di, J.; Xu, L.; Zhu, X. Reinforcing effect of nanocrystalline cellulose and office waste paper fibers on mechanical and thermal properties of poly (Lactic Acid) composites. *J Appl Polym Sci* 2021, 138, doi:10.1002/app.50462.
63. Szebényi, G.; Hliva, V. Detection of delamination in polymer composites by digital image correlation-experimental test. *Polymers (Basel)* 2019, 11, doi:10.3390/polym11030523.
64. Aravind, T.; Ashraf, M.S.; A. S, R.; Ahalya, N.; Rawat, M.S.; Uma, B.; Sharma, R.; Subbiah, R.; Sida, S. Study of progress on nanocrystalline cellulose and natural fiber reinforcement biocomposites. *J Nanomater* 2022, 2022, doi:10.1155/2022/6519480.
65. Cerbu, C.; Ursache, S.; Botis, M.F.; Hadăr, A. Simulation of the hybrid carbon-aramid composite materials based on mechanical characterization by digital image correlation method. *Polymers (Basel)* 2021, 13, doi:10.3390/polym13234184.
66. Suarez, S.A.; Gibson, R.F.; Sun, C.T.; Chaturvedi, S.K. The influence of fiber length and fiber orientation on damping and stiffness of polymer composite materials. *Exp Mech* 1986, 26, 175–184, doi:10.1007/BF02320012.
67. Cieszyński, T.; Topoliński, T. Badania zmęczeniowe kompozytów polimerowych przy sterowaniu energią dyssypacji. *czasopismo techniczne. Mechanika -WPK. Mechanika* 2006, 103, 115–119.
68. Mazurkiewicz, S.; Porębska, R. Energia dyssypacji w kompozytach polimerowych. *czasopismo techniczne. Mechanika -WPK* 2009, 106, 245–248.
69. Kaczor, P.; Bazan, P.; Kuciel, S. Bioactive polyoxymethylene composites : mechanical and antibacterial characterization. *Materials* 2023, 16, 5718.
70. Bazan, P.; Ewelina, K.; Rybicka, K. Industrial crops & products the influence of organic and inorganic antibacterial additives on the strength and biocidal properties of thermoplastic elastomers (TPO). 2023, 198, doi:10.1016/j.indcrop.2023.116682.
71. Panin, S. V.; Bogdanov, A.A.; Eremin, A. V.; Buslovich, D.G.; Alexenko, V.O. Estimating low-and high-cyclic fatigue of polyimide-CF-PTFE composite through variation of mechanical hysteresis loops. *Materials* 2022, 15, doi:10.3390/ma15134656.
72. Dong, W.; Huang, C.; Wang, Y.; Sun, Y.; Ma, P.; Chen, M. Superior mechanical properties of double-network hydrogels reinforced by carbon nanotubes without organic modification. *Int J Mol Sci* 2013, 14, 22380–22394, doi:10.3390/ijms141122380.
73. Webber, R.E.; Creton, C.; Brown, H.R.; Gong, J.P. Large strain hysteresis and mullins effect of tough double-network hydrogels. *Macromolecules* 2007, 40, 2919–2927, doi:10.1021/ma062924y.
74. Krasnobrizha, A.; Rozycki, P.; Gornet, L.; Cosson, P. Hysteresis behaviour modelling of woven composite using a collaborative elastoplastic damage model with fractional derivatives. *Compos Struct* 2016, 158, 101–111, doi:10.1016/j.compstruct.2016.09.016.
75. Luo, X.; Chen, Q.; Deng, C.; Luo, W.; He, Y. Low-cyclic reversed loading tests on full-scale precast concrete composite wall connected by tooth groove and grouted sleeve. *Materials* 2024, 17, doi:10.3390/ma17020476.
76. Connesson, N.; Maquin, F.; Pierron, F. Dissipative Energy as an Indicator of Material Microstructural Evolution. *EPJ Web Conf* 2010, 6, 1–6, doi:10.1051/epjconf/20100638013.
77. Scott-Emuakpor, O.E.; George, T.J.; Cross, C.J.; Shen, M.H.H. Analysis of strain energy behavior throughout a fatigue process. *Exp Mech* 2011, 51, 1317–1323, doi:10.1007/s11340-010-9457-9.
78. Ospina Cadavid, M.; Al-Khudairi, O.; Hadavinia, H.; Goodwin, D.; Liaghat, G.H. Experimental studies of stiffness degradation and dissipated energy in glass fibre reinforced polymer composite under fatigue loading. *Polymers and Polymer Composites* 2017, 25, 435–446, doi:10.1177/096739111702500602.
79. Risitano, A.; La Rosa, G.; Geraci, A.; Guglielmino, E. The choice of thermal analysis to evaluate the monoaxial fatigue strength on materials and mechanical components. *Proc Inst Mech Eng C J Mech Eng Sci* 2015, 229, 1315–1326, doi:10.1177/0954406215572429.
80. Marat-Mendes, R.; Rodrigues, I.; Figueiredo-Pina, C.G. Evaluation of tribological performance of carbon fibre reinforced epoxy composites loaded with graphite platelets under reciprocating linear motion. *Proceedings of the Institution of Mechanical Engineers, Part J: Journal of Engineering Tribology* 2019, 233, 1415–1423, doi:10.1177/1350650119826443.
81. Khammassi, S.; Tarfaoui, M. Influence of exfoliated graphite filler size on the electrical, thermal, and mechanical polymer properties. *J Compos Mater* 2020, 54, 3731–3741, doi:10.1177/0021998320918639.
82. Mousa, A.; Heinrich, G.; Wagenknecht, U.; Arabayat, O. The effect of exfoliated graphite on the thermal and mechanical properties of dynamically vulcanized polystyrene/styrene butadiene rubber composites. *J Eng Mater Technol* 2018, 140, 011003.

83. Gately, N.M.; Kennedy, J.E. Processing stability and the significance of variation in extrusion speeds and temperatures on SSB® 55 Pharma Grade Shellac for oral drug delivery. *Journal of Manufacturing and Materials Processing* 2017, 1, 1–14, doi:10.3390/jmmp1010009.
84. Lin, Y.; Kouznetsova, T.B.; Chang, C.C.; Craig, S.L. Enhanced polymer mechanical degradation through mechanochemically unveiled lactonization. *Nat Commun* 2020, 11, 1–10, doi:10.1038/s41467-020-18809-7.
85. Zhou, J.; Hsu, T.G.; Wang, J. mechanochemical degradation and recycling of synthetic polymers. *Angewandte Chemie - International Edition* 2023, 62, doi:10.1002/anie.202300768.
86. Miller, K.A.; Morado, E.G.; Samanta, S.R.; Walker, B.A.; Nelson, A.Z.; Sen, S.; Tran, D.T.; Whitaker, D.J.; Ewoldt, R.H.; Braun, P. V.; et al. Acid-triggered, acid-generating, and self-amplifying degradable polymers. *J Am Chem Soc* 2019, 141, 2838–2842, doi:10.1021/jacs.8b07705.
87. Tu, Y.; Chen, J.; Wang, S.; Wang, W. Moisture migration in oil-impregnated film insulation under thermal ageing. *IEEE Transactions on Dielectrics and Electrical Insulation* 2016, 23, 1135–1141, doi:10.1109/TDEI.2015.005406.
88. Sadritdinov, A.R.; Chernova, V. V.; Bazunova, M. V.; Zakharova, E.M.; Zakharov, V.P. Strength characteristics of polymer composites based on recycled polypropylene filled with rice husk during moisture absorption and natural aging. *Periodico Tche Quimica* 2020, 17, 845–855, doi:10.52571/ptq.v17.n36.2020.860_periodico36_pgs_845_855.pdf.
89. Tue recycle of plastic waste and agricultural waste. *Energy Research Journal* 2013, 4, 24–29, doi:10.3844/erj.2013.24.29.
90. Zhao, J.; Li, Q.; Li, S.; Li, S.; Chen, G.; Liu, X.; He, Y.; Luo, J. Influence of a carbon-based tribofilm induced by the friction temperature on the tribological properties of impregnated graphite sliding against a cemented carbide. *Friction* 2021, 9, 686–696, doi:10.1007/s40544-019-0358-3.
91. Hubert, P.J.; Kathiresan, K.; Wakabayashi, K. Filler exfoliation and dispersion in polypropylene/as-received graphite nanocomposites via cryogenic milling. *Polym Eng Sci* 2011, 51, 2273–2281, doi:10.1002/pen.
92. Alshammari, B.A.; Al-Mubaddel, F.S.; Karim, M.R.; Hossain, M.; Al-Mutairi, A.S.; Wilkinson, A.N. Addition of graphite filler to enhance electrical, morphological, thermal, and mechanical properties in poly (Ethylene Terephthalate): Experimental characterization and material modeling. *Polymers (Basel)* 2019, 11, 1–20, doi:10.3390/polym11091411.
93. Płaza, S.; Margielewski, L.; Celichowski, G. Wstęp do tribologii i tribochemia; Wydawnictwo Uniwersytetu Łódzkiego: Łódź, 2005.
94. Walczak, M.; Szala, M.; Pieniak, D. Effect of water absorption on tribological properties of thermoplastics matrix composites reinforced with glass fibres. *Advances in Science and Technology Research Journal* 2022, 16, 232–239, doi:10.12913/22998624/147515.
95. Rymuza, Z. *Trybologia Polimerów Ślizgowych*; Wydawnictwo Naukowo-Techniczne: Warszawa, 1986;
96. Jin, H.; Zhou, K.; Ji, Z.; Tian, X.; Chen, Y.; Lu, L.; Ren, Y.; Xu, C.; Duan, S.; Li, J.; et al. Comparative tribological behavior of friction composites containing natural graphite and expanded graphite. *Friction* 2020, 8, 684–694, doi:10.1007/s40544-019-0293-3.
97. Xue, Y.; Yan, S.; Chen, Y. Thermomechanical and tribological properties of polyimide and polyethersulfone blends reinforced with expanded graphite particles at various elevated temperatures. *J Appl Polym Sci* 2022, 139, doi:10.1002/app.52512.
98. Lo, T.; Kuo, W.; Cheng, C. Material Characterization of graphite nanosheet composites. *Polym Compos* 2011, 32, 305–313, doi:10.1002/pc.21051.
99. Yan, S.; Yang, Y.; Song, L.; Qi, X.; Xue, Y.; Duan, C. Tribological behavior of graphite oxide reinforced polyethersulfone composite under drying sliding condition. *Polym Compos* 2018, 39, 2320–2335, doi:10.1002/pc.24211.
100. Panin, S. V.; Luo, J.; Buslovich, D.G.; Alexenko, V.O.; Kornienko, L.A.; Bochkareva, S.A.; Byakov, A. V. Experimental—FEM study on effect of tribological load conditions on wear resistance of three-component high-strength solid-lubricant PI-based composites. *Polymers (Basel)* 2021, 13, 2837, doi:10.3390/polym13162837.
101. Shang, Y.; Zhao, Y.; Liu, Y.; Zhu, Y.; Jiang, Z.; Zhang, H. The effect of micron-graphite particle size on the mechanical and tribological properties of PEEK composites. *High Perform Polym* 2018, 30, 153–160, doi:10.1177/0954008316685410.
102. You, Y.-L.; Li, D.-X.; Deng, X.; Li, W.-J.; Xie, Y. Effect of solid lubricants on tribological behavior of glass fiber reinforced polyamide 6. *Polymer Composites* 2013, 34, 1783–1793, doi:10.1002/pc.
103. Alajmi, M.; Shalwan, A. Correlation between mechanical properties with specific wear rate and the coefficient of friction of graphite/epoxy composites. *Materials* 2015, 8, 4162–4175, doi:10.3390/ma8074162.
104. Katiyar, J.K.; Sinha, S.K.; Kumar, A. Effects of carbon fillers on the tribological and mechanical properties of an epoxy-based polymer (SU-8). *Tribology - Materials, Surfaces and Interfaces* 2016, 10, 33–44, doi:10.1080/17515831.2015.1126689.
105. Sakka, M.M.; Antar, Z.; Elleuch, K.; Feller, J.F. Tribological response of an epoxy matrix filled with

- graphite and/or carbon nanotubes. *Friction* 2017, 5, 171–182, doi:10.1007/s40544-017-0144-z.
106. Przekop, R.E.; Kujawa, M.; Pawlak, W.; Dobrosielska, M.; Sztorch, B.; Wieleba, W. Graphite modified polylactide (PLA) for 3D printed (FDM/FFF) sliding elements. *Polymers (Basel)* 2020, 12, 1–22, doi:10.3390/POLYM12061250.
107. Feng, C.; Ni, H.; Chen, J.; Yang, W. Facile method to fabricate highly thermally conductive graphite/PP composite with network structures. *ACS Appl Mater Interfaces* 2016, 8, 19732–19738, doi:10.1021/acsami.6b03723.
108. Guo, H.X.; Yang, J.F. Fabrication and Tribological Properties of Mesocarbon Microbead-Cu Friction Composites. *Materials* 2020, 13, doi:10.3390/ma13020463.
109. Jin, H.; Zhou, K.; Ji, Z.; Tian, X.; Chen, Y.; Lu, L.; Ren, Y.; Xu, C.; Duan, S.; Li, J.; et al. Comparative tribological behavior of friction composites containing natural graphite and expanded graphite. *Friction* 2020, 8, 684–694, doi:10.1007/s40544-019-0293-3.
110. Katiyar, J.K.; Sinha, S.K.; Kumar, A. Effect of graphite concentration on the tribological and mechanical properties of filled SU-8 polymer. *Tribology Online* 2016, 11, 152–158, doi:10.2474/trol.11.152.